Journal of Electroceramics, 13, 281–286, 2004

Microwave Dielectric Mechanism Studied by Microwave Near-Field Microscopy and Raman Spectroscopy

YI-CHUN CHEN[1,2,*], YEONG-DER YAO[2], YUN-SHUO HSIEH[1], HSIU-FUNG CHENG[*,1], CHIH-TA CHIA[1] & I-NAN LIN[3]

[1]*Department of Physics, National Taiwan Normal University, Taipei 116, Taiwan, Republic of China*
[2]*Institute of Physics, Academia Sinica, Taipei 115, Taiwan, Republic of China*
[3]*Department of Physics, Tamkang University, Tamsui 251, Taiwan, Republic of China*

Submitted March 28, 2003; Revised February 7, 2004; Accepted May 17, 2004

Abstract. Microwave dielectric ceramics such as $Ba(Mg_{1/3}Ta_{2/3})O_3$ and $Ba_2Ti_9O_{20}$ possess high dielectric constant and low dielectric loss in microwave frequency regime and have tremendous potential for device applications. In these materials, the presence of extrinsic defects, such as secondary phases, usually altered the microwave dielectric properties of the materials markedly, but the correlation of the microwave dielectric response of the materials with their microstructure has not been fully understood due to the lack of dielectric response in the local area. In this article, microwave near-field microscopy and Raman spectroscopy were used to investigate the microwave dielectric mechanism, viz. we measured the microwave dielectric properties of the materials in micron region by using a evanescent microwave probe (EMP) and, at the same time, examined the lattice vibration characteristics of the region by using a micro-Raman spectrum. How the presence of the secondary phase affects the microwave dielectric properties of the materials is thus systematically investigated. The causes of intrinsic or extrinsic dielectric loss were explored by comparing the dielectric images in SEMP at microwave frequencies and the corresponding Raman Spectra.

Keywords: Evanescent microwave microscopy, microwave dielectrics, Raman spectroscopy

1. Introduction

Generally, the dielectric losses in microwave dielectrics, which reduce the quality factor (Q-factor), could be induced either intrinsically or extrinsically. The intrinsic factors are related to material composition and crystal structure, which are less process dependent, whereas the extrinsic factors are related to defects (vacancies, impurities), structural disorder, porosity or second phases... etc., which are more process dependent. The most promising approach to understand the intrinsic microwave dielectric properties of the materials is to study their higher frequency response, including the submillimeter and infrared regime [1–4], since the intrinsic losses are overwhelmingly stronger than the extrinsic ones in the far-infrared regime. By contrast, extrinsic loss is usually obvious in the dielectric measurement at microwave frequencies. High Q-factor is of the most concern. Among the microwave dielectrics, the $BaO\text{-}TiO_2$ [5–7] system and complex perovskites [8–10] with general formula $A(B_{1/3}B'_{2/3})O_3$, where $A = Ba^{2+}$, $B = Mg^{2+}, Zn^{2+}$ or Ni^{2+}, $B' = Ta^{5+}$ or Nb^{5+} possess an excellent combination of high quality factor (Q), moderate dielectric constant (K), and low temperature coefficient of resonant frequency (τ_f) in the microwave frequency region. Therefore, these materials are commonly used as resonators in microwave devices and investigated in this study.

To examine the microwave properties of extrinsic defects in micrometer scale, the development of high-resolution microscope that can probe dielectric properties at microwave frequencies is needed. The classical

*To whom all correspondence should be addressed. E-mail: hfcheng@phy03.phy.ntnu.edu.tw

limit to the spatial resolution of any instrument based on the propagation of electromagnetic fields is $\lambda/2$, which turns into the main difficulty of getting a microwave microscopeu However, evanescent waves, which decay exponentially in a propagation electromagnetic wave of wavelength λ, have spatial frequency components higher than $1/\lambda$, and have been used in near-field microscopy to achieve a spatial resolution of $\lambda/20$–$\lambda/60$ at different wavelengths. In this article, an evanescent microwave probe (EMP) based on a microwave resonator [11–13] is proposed to image surface impedance profiles in microwave frequency region, while Raman spectroscope was used to examine intrinsic properties of $Ba(Mg_{1/3}Ta_{2/3})O_3$ series samples.

2. Experimental Methods

$Ba_2Ti_9O_{20}$ (B_2T_9) materials were prepared by the coprecipitation method while $Ba(Mg_{1/3}Ta_{2/3})O_3$ (BMT) materials were also prepared by conventional mixed-oxide process. To synthesize B_2T_9, the $Ba(OH_2)\cdot 2H_2O$ and $TiCl_4$ with appropriate ratio (Ba:Ti = 2:9) were dissolved in H_2O, which were then spread into coprecipitants consisting of $NH_4(OH)$ and $(NH_4)_2CO_3$ mixture. The coprecipitates thus obtained were then filtered and washed for several times to get rid of residual NH_4Cl. The coprecipitates were then calcined at 1100°C for 4 h, followed by pulverization, pressing and then sintered at 1300°C for 4 h (in air). The BMT materials were synthesized by directly calcining the $BaCO_3$, MgO and Ta_2O_5 powder mixture of 3 : 1 : 2 molar ratio, followed by pulverization, pelletization and then sintering at 1550°C for 4 h.

The crystal structure and microstructure of the sintered samples were examined using X-ray diffraction and scanning electron microscopy. The average microwave dielectric properties of the materials were measured using the conventional cavity method. To investigate the local variation of dielectric properties of the materials, an evanescent microwave probe (EMP) was used to make nondestructive measurements of the dielectric properties of the samples. The system design consists of a sharpened metal tip, mounted on the center conductor of a high-Q (quality factor) $\lambda/4$ coaxial resonator, protruding beyond an aperture formed on the end wall of the resonator. A change in the local environment of the probe leads to a change in the resonant frequency f_0 of the resonator, and the signal is detected by measuring the power response near the resonant frequency. Contact mode is used during the scanning because it possesses higher sensitivity and is easier for electromagnetic field analysis. To perform quantitative measurements, perturbation theory was used to analyze the resonant system. From the shift of resonant frequencies (Δf) and the change in resonator's Q-value ($\Delta\frac{1}{Q}$), the dielectric properties of the bulk sample can be analyzed by the following equations [13]:

$$\frac{\Delta f}{f_0} = -\frac{\int_v (\Delta\varepsilon E_1 \cdot E_0 + \Delta\mu H_1 \cdot H_0)dv}{\int_v \left(\varepsilon_0 E_0^2 + \mu_0 H_0^2\right)dv} = A\left[\frac{\ln(1-b)}{b} + 1\right] \tag{1}$$

$$\Delta\left(\frac{1}{Q}\right) = -\frac{\int_v (\Delta\varepsilon'' E_1 \cdot E_0 + \Delta\mu'' H_1 \cdot H_0)dv}{\int_v \left(\varepsilon_0 E_0^2 + \mu_0 H_0^2\right)dv} = -\left(\frac{1}{Q_0} + 2\tan\delta\right)\frac{\Delta f}{f_0} \tag{2}$$

where $\vec{E_0}$, $\vec{H_0}$ and $\vec{E_1}$, $\vec{H_1}$, refer to the electric and magnetic field before and after perturbation, respectively; $\Delta f = f_r - f_0$ and $\Delta(\frac{1}{Q}) = \frac{1}{Q} - \frac{1}{Q_0}$, where f_0 and Q_0 are the resonant frequency and quality factor of the resonator without the samples, while f_r and Q_r are the measured resonant frequency and quality factor of the resonator with a sample placed adjacent to the EMP probe; $b = \frac{\varepsilon-\varepsilon_0}{\varepsilon+\varepsilon_0}$, where ε is the dielectric constant of the sample, ε_0 is the permittivity of free space, and A is a constant determined by the geometry of the tip-cavity assembly which should be calibrated using standard samples. With a proper design, the far-field background signal can be minimized and the submicron spatial resolution is obtained.

Meanwhile, a DILOR XY 800 triple-grating Raman spectrometer equipped with a liquid-nitrogen-cooled CCD was used for micro-Raman spectrum measurements. The 514.5 nm line of an Ar^+ ion laser with output 10 mW was used as the excitation source and Olympus BH-2 microscope with 100× objective was employed for room temperature micro-Raman spectrum detection. The recorded Raman spectra exhibit approximately 1 cm^{-1} resolution.

3. Results and Discussions

Microwave dielectric responses of a material are mostly determined by its intrinsic properties, such as crystal structures and polarization mechanism. However, it is

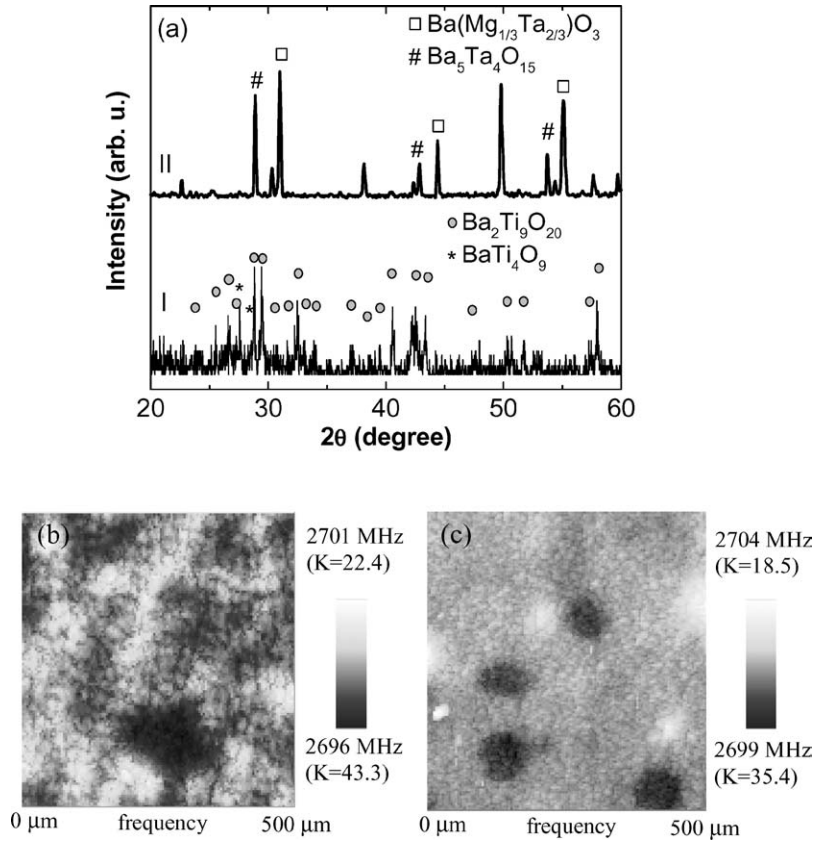

Fig. 1. (a) X-ray diffraction patterns of the tested (I) $Ba_2Ti_9O_{20}$ and (II) $Ba(Mg_{1/3}Ta_{2/3})O_3$ samples; frequency images of the (b) $Ba_2Ti_9O_{20}$ and (c) $Ba(Mg_{1/3}Ta_{2/3})O_3$ samples scanned by EMP method.

usually observed that different synthesis processes result in various properties of the materials. Therefore, the extrinsic factors, which influence the dielectric properties of the material, also need to be investigated. The effect of secondary phases and defects on the microwave properties can be revealed by investigating BMT and B_2T_9 ceramics as examples. Figure 1(a) shows that the tested BMT and B_2T_9 samples are readily crystallized, but the pure BMT perovskite phase and B_2T_9 hollandite phases are not obtained. The phase purity for the sintered B_2T_9 materials is closely related to phase constituent in the as-calcined powders. The $BaTi_5O_{11}$ phase was preferentially formed when the $BaCO_3$-TiO_2 mixture was calcined at 1100°C, and most of the intermediate phase can be converted into the hollandite structure by sintering at 1300°C for 4 h. X-ray diffraction pattern [Fig. 1(a)-I] shows that the as obtained B_2T_9 ceramics contain a large proportion of second phases, mainly the $BaTi_4O_9$ intermediate phase. Similarly, second phases, mainly the $Ba_5Ta_4O_{15}$ phase, are easily induced when the BMT samples are synthesized directly by mixed-oxide process [Fig. 1(a)-II]. The dielectric properties of the samples are intimately correlated with their phase purity. The microwave properties were markedly degraded for the 1100°C-derived B_2T_9, with dielectric constant $K = 32.3$, and quality factor $Q \times f = 13,900$ GHz, as compared with those of our pure B_2T_9 samples or referenced data, $K \sim 40$, $Q \times f \sim 36{,}000$ GHz [5–7]. Pure BMT samples also have better dielectric properties ($K \sim 26$, $Q \times f \sim 100{,}000$ GHz) [9, 10] than the samples containing second phase ($K \sim 24.8$, $Q \times f \sim 48{,}000$ GHz).

To obtain the image of dielectric properties of each microstructure feature in microwave regime, EMP was used to map the dielectric properties of the ceramics. The measurement is based on the principle that as the tip approaches the sample surface, the evanescent wave

from the tip of a resonator will interact with the sample, inducing the field redistribution. This effect can be modeled by adding additional capacitive impedance to the resonator, which causes the shift of resonant frequency. Figures 1(b) and (c) show the frequency mappings of the B_2T_9 and BMT samples, respectively. The dielectric constant analyzed from the resonant frequency by using Eqs. (1) and (2) are also indicated in these figures. In addition to the main matrices, both Figs. 1(b) and (c) possess some strange regions with higher or lower dielectric constants, in accordance with the existence of second phases in these samples. These mappings reveal that the average dielectric constant for B_2T_9 sample is around 32–33 while the average dielectric constant for the BMT sample is around 25–26. This phenomenon is quite consistent with dielectric properties measured by conventional cavity method.

The dielectric images of the low-K areas on the B_2T_9 and BMT samples examined using EMP high-resolution modes are shown in Figs. 2(a) and (b), respectively. The dielectric constant varies pronouncedly over this region. Grains with low dielectric constant (or high resonant frequency) aggregate, forming clusters typically tens of microns in size. In B_2T_9 image [Fig. 2(a)], the low dielectric constant region contains several equiaxed clusters about tens of microns, and the high dielectric constant region consists of needle-like clusters, about 1 μm in diameter and several tens of microns in length. Most probably the needle-like clusters are $Ba_2Ti_9O_{20}$ grains, whereas the equiaxed clusters are secondary phases. In contrast, the fluctuation of dielectric constants for the clusters in Fig. 2(b) can be attributed to the presence of a large proportion of $Ba_5Ta_4O_{15}$ secondary phase. Compared with the SEM images (not shown), the matrices, i.e., polygonal clusters, are BMT grains, while the elongated clusters are $Ba_5Ta_4O_{15}$ secondary phases. Regions of extremely low dielectric constant were observed all over the B_2T_9 and BMT samples, which is presumably the factor resulting in the markedly lower average dielectric constant for these materials.

To further investigate the extrinsic dielectric mechanism of the materials, the EMP measurement was correlated with a micro-Raman spectrum measurement. Since the correlation of the microwave properties and lattice vibrational modes for BMT complex perovskite has been unambiguously performed recently [4, 14], the mapping of EMP resonant frequency and micro-Raman spectrum intensity for a high-dielectric-constant (low-resonant-frequency) region of BMT

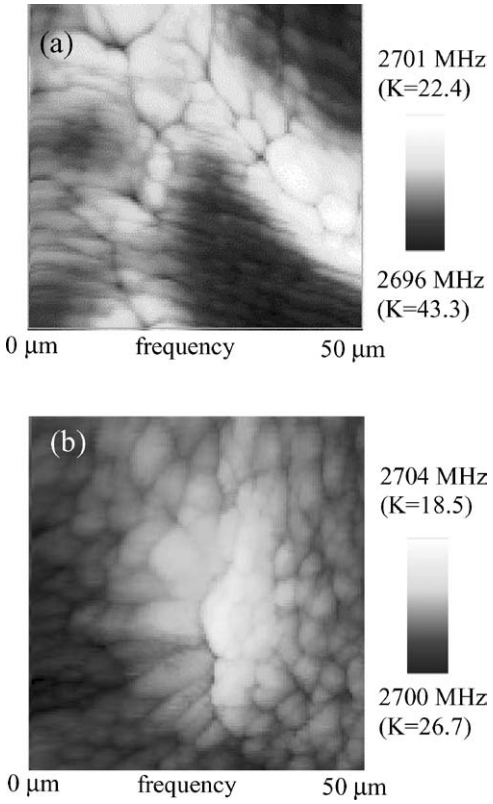

Fig. 2. Enlarged frequency images for the second phase region in (a) $Ba_2Ti_9O_{20}$ and (b) $Ba(Mg_{1/3}Ta_{2/3})O_3$ samples, scanned by EMP method.

were investigated simultaneously [Figs. 3(a) and (b)]. The spatial resolution achievable in EMP measurement is about sub-micrometer, which is higher than that in micro-Raman spectrum, so we can see more detailed structure in Fig. 3(a). Figure 3(a) reveals that the shape of the grains in this region is not much different from the granular grains in normal region, but the dielectric constants in this region are pronouncedly higher than others. Figure 3(b) show that the mapping of the Raman intensity for TaO_6 breathing mode (A_{1g}[O], 788 cm^{-1}) is strongly correlated with microwave response measured by EMP. As shown in Fig. 4(a), the A_{1g}[O] breathing mode is related to the rigidity of $B'O_6$ octahedra in complex perovskite, which dominates the polarization mechanism contributing to the dielectric response at microwave frequencies [4, 14]. It should be noted that the contrast observed in Fig. 3(a) to (b) is mainly due to the defects in crystal structure rather than in topology, as the optical microscopic image in Fig. 3(c) shows no similar correlations.

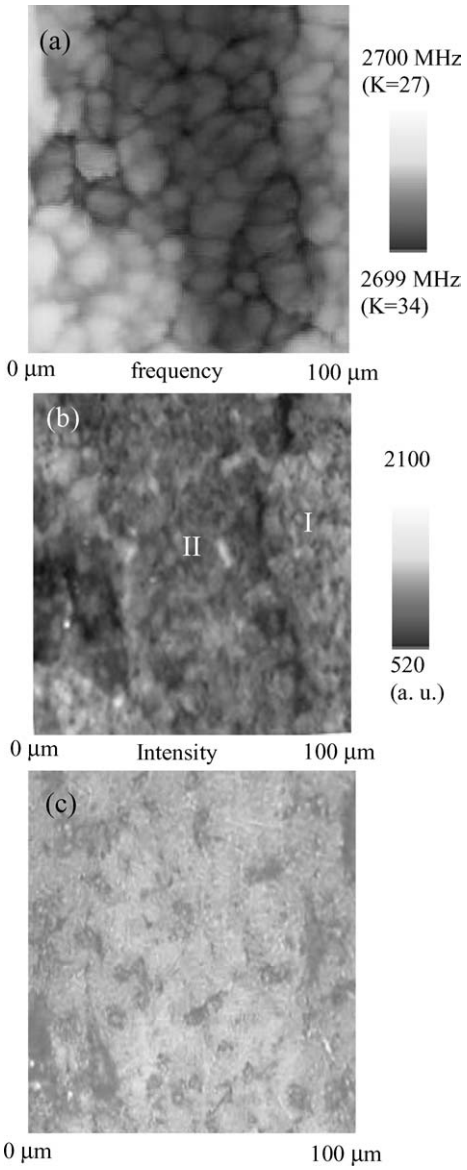

Fig. 3. Surface images of BMT ceramics taken by (a) evanescent microwave probe, (b) scanning Raman microscope, and (c) optical microscope.

Typical Raman spectra for low-K region (labeled as I) and high-K region (labeled as II) are illustrated in Fig. 4(b). The Raman signals in region II are of much lower intensity than that in region I, indicating that the region II contains some un-crystallized materials (or the phases other than perovskite), which is presumed to be the factor resulting in larger loss factor for the region II materials. The large damping coefficient in region II is most probably due

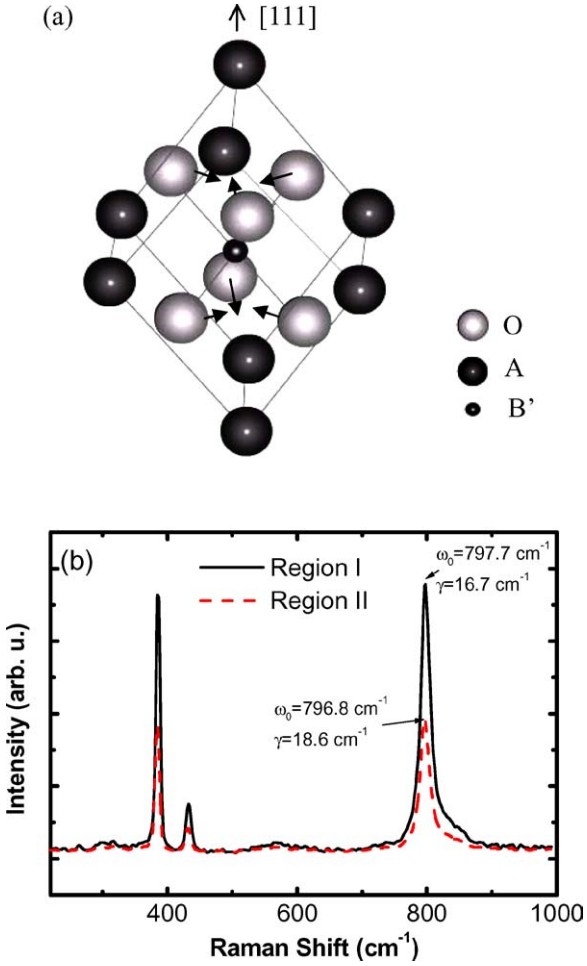

Fig. 4. (a) Illustration of $A_{1g}[O]$ breathing mode in BMT complex perovskite and (b) micro Raman spectra of BMT measured in high-K region (I) and low-K region (II) of Fig. 3.

to the distortion of the grains in this region. Resonant peaks with strong intensity around 385 cm^{-1}, 437 cm^{-1}, and 797 cm^{-1} are unambiguously assigned as $A_{1g}[O] + E_g[O]$, $E_g[O]$, and $A_{1g}[O]$ vibrational modes, respectively [14]. Among these modes, the $A_{1g}[O]$ mode around 797 cm^{-1} is the breathing vibration of TaO_6 octahedron, and is especially significantly correlated with the microwave properties [14]. Figure 4(b) shows the breathing mode around 797 cm^{-1} for region II materials slightly red shift, as compared with that for region I materials. The implication for this phenomenon is that the Ta─O bond strength in region II materials is weaker, which results in larger polarizability and hence higher dielectric constant for region II materials.

4. Conclusions

To realize the extrinsic dielectric mechanism at microwave frequencies, the dielectric constants $Ba_2Ti_9O_{20}$ (B_2T_9), and $Ba(Mg_{1/3}Ta_{2/3})O_3$ (BMT) ceramics were measured at microwave frequencies directly using an evanescent microwave probe (EMP) technique. The EMP images reveal the distribution of dielectric properties in the bulk materials, which is consistent with XRD crystal structure examinations. The average dielectric constants derived from EMP measurements are in good agreement with results obtained by conventional cavity method. EMP images reveal that the samples with inferior dielectric properties usually contain a large proportion of low-K and low-Q secondary phase, which is the main cause degrading the microwave dielectric properties. Moreover, the results shown in EMP dielectric image and micro-Raman phonon-intensity image indicate that the grains with distorted crystal structure, which show higher dielectric constants and larger losses, can also act as extrinsic defects for ceramic materials.

Acknowledgment

Financial support of National Science Council, R. O. C., through the projects no. NSC 91-2622-E-007-032, NSC 91-2112-M-003-024 and NSC 92-2622-E-007-016, NSC 92-2218-E-003-001 is gratefully acknowledged by the authors.

References

1. J. Petzelt, S. Kamba, G.V. Kozlov, and A.A. Volkov, *Ferroelectrics*, **176**, 145 (1996).
2. J. Petzelt and N. Setter, *Ferroelectrics*, **150**, 89 (1993).
3. K. Wakino, M. Murata, and H. Tamura, *J. Am. Ceram. Soc.*, **69**(1), 34 (1986).
4. Y.C. Chen, H.F. Cheng, H.L. Liu, C.T. Chia, and I.N. Lin, *J. Appl. Phys.*, **94**(6), 1 (2003).
5. J.K. Plourde, D.F. Linn, H.M. O'Bryan, Jr., and J. Thomson, Jr., *J. Am. Ceram. Soc.*, **58**, 418 (1975).
6. J.H. Choy and Y.S. Han, *J. Am. Ceram. Soc.*, **78**, 1169 (1995).
7. W.Y. Lin and R.F. Speyer, *J. Am. Ceram. Soc.*, **82**, 1207 (1999).
8. S.B. Desu and H.M. O'Bryan, *J. Am. Ceram. Soc.*, **68**(10), 546 (1985).
9. S. Nomura, K. Toyama, and K. Kaneta, *Jpn. J. Appl. Phys. Part 2*, **21**, L624 (1982).
10. R. Guo, A.S. Shalla, and L.E. Cross, *J. Appl. Phys.*, **75**, 4704 (1994).
11. Y. Lu, T. Wei, F. Duewer, Y. Lu, N.B. Ming, P.G. Schultz, and X.D. Xiang, *Science*, **276**, 2004 (1997).
12. G. Chen, T. Wei, F. Duewer, Y. Lu, and X.D. Xiang, *Appl. Phys. Lett.*, **71**, 1872 (1997).
13. C. Gao, F. Duewer, and X.D. Xiang, *Appl. Phys. Lett.*, **75**, 3005 (1999).
14. C.T. Chia, Y.C. Chen, H.F. Cheng, and I.N. Lin, *J. Appl. Phys.*, **94**, 3360 (2003).